Crystal structure of soybean 11S globulin: Glycinin A3B4 homohexamer

Motoyasu Adachi*, Jiro Kanamori[†], Taro Masuda*, Kazuhiro Yagasaki[‡], Keisuke Kitamura[§], Bunzo Mikami*, and Shigeru Utsumi*[¶]

*Laboratory of Food Quality Design and Development, Graduate School of Agriculture, Kyoto University, Uji, Kyoto 611-0011, Japan; [†]Fuji Oil Co., Ltd., Ibaraki 300-2497, Japan; [‡]Nagano Chushin Agricultural Experiment Station, Shiojiri, Nagano 399-6461, Japan; and [§]National Agricultural Research Organization, Tsukuba, Ibaraki 305-8517, Japan

Most plant seeds contain 11S globulins as major storage proteins for their nutrition. Soybean glycinin belongs to the 11S globulin family and consists of five kinds of subunits. We determined the crystal structure of a homohexamer of the glycinin A3B4 subunit at 2.1-Å resolution. The crystal structure shows that the hexamer has 32-point group symmetry formed by face-to-face stacking of two trimers. The interface buries the highly conserved interchain disulfide. Based on the structure, we propose that an ingenious face-to-face mechanism controls the hexamer formation of the 11S globulin by movement of a mobile disordered region to the side of the trimer after posttranslational processing. Electrostatic analysis of the faces suggests that the interchain disulfide-containing face has high positive potential at acidic pH, which induces dissociation of the hexamer into trimers that may be susceptible to proteinases after seed imbibition. This dissociation might result in the degradation and mobilization of 11S globulins as storage proteins in embryos during germination and seedling growth.

Plants accumulate protein reserves in developing seeds to act as a sink of nitrogen, sulfur, and carbon. Most dicotyledonous plant seeds contain 7S and/or 11S globulins and albumins as the major storage proteins in the embryo or cotyledons, whereas some cereals such as wheat, barley, and corn contain prolamins in the endosperm (1, 2). The 11S globulins are distributed more widely than the 7S globulins among plant seeds. Although the quaternary structures of the 7S and 11S globulins are different from each other (the former being a trimeric protein and the latter a hexameric protein), they are believed to be derived from a common ancestor because of the partial homologies in their amino acid sequences and limited proteolysis patterns (3). This assumption has been confirmed by x-ray crystallography of 7S globulins from kidney bean (4), jack bean (5), and soybean (6) and of the trimeric soybean 11S globulin precursor (7).

In general, 11S globulins are composed of several kinds of subunits. For example, five major subunits have been identified from soybean: A1aB1b, A2B1a, A1bB2, A3B4, and A5A4B3. In developing seeds, the constituent subunits of 11S globulin are synthesized as a single polypeptide precursor, preproprotein, the signal sequence of which is removed cotranslationally. The resultant proproteins assemble into trimers of ≈8S in the endoplasmic reticulum. The proprotein trimers are transported from the endoplasmic reticulum to protein storage vacuoles (PSVs), where they then are cleaved to form acidic and basic polypeptides that are linked by a disulfide bond (8). Finally, the mature proteins assemble into hexamers. The protein reserves are stored in the dormant seed until its germination.

Recently we determined the crystal structure of the soybean proglycinin A1aB1b homotrimer at 2.8-Å resolution (7). The protomer consists of N- and C-terminal modules that each include a jelly-roll β-barrel and a helix domain. However, the packaging of the trimers in the hexamer is not known, because it is very difficult to obtain crystals of 11S globulin suitable for x-ray analysis because of their molecular heterogeneity. Here we report the crystal structure of the glycinin A3B4 homohexamer

purified from a mutant soybean cultivar containing glycinin composed of only the A3B4 subunit (9). In addition, we reveal what happens after the cleavage of the proglycinin to the mature glycinin and how the trimers stack to form the hexamer.

Methods

Protein Purification and Crystallization. Glycinin A3B4 homohexamer was purified from a mutant soybean cultivar containing glycinin composed of only A3B4 subunit (9). The protein was extracted with a buffer of 10 mM Tris (pH 8.0) containing 10 mM 2-mercaptoethanol, 1 mM EDTA, and 0.1 mM p-aminophenyl methanesulfonyl fluoride hydrochloride (p-APMSF). The pH of the extract was adjusted to 6.4 by HCl at 4°C. After centrifugation at $5,000 \times g$, the precipitate was dissolved in 35 mM potassium phosphate buffer (pH 7.6) containing 0.4 M NaCl, 10 mM 2-mercaptoethanol, and 0.1 mM p-APMSF. The protein was fractionated by ammonium sulfate from 50% to 65% saturation and purified by using a Q-Sepharose HiLoad 26/10 column (Amersham Pharmacia). The purified protein solution was dialyzed against 35 mM potassium-phosphate buffer (pH 7.6) containing 1 M NaCl, 10 mM 2-mercaptoethanol, and 0.02% NaN$_3$. Crystals were obtained according to the method of Kanamori *et al.*[‖] Briefly, 80 μl of protein solution (20 mg·ml^{-1}) was mixed with 80 μl of Mes buffer (pH 4.0) and 29 μl of 2-methyl-2,4 pentandiol, and the mixed solution was kept for 5 months in VIAL MV-03 (As One Co., Osaka) at 20°C.

Data Collection, Structure Determination, and Refinement. X-ray diffraction data were collected at room temperature by using CuKα radiation with a Bruker (Billerica, MA) Hi-Star area detector coupled to a Bruker AXS (Yokohama, Japan) M18XHF rotating anode generator. The crystal belongs to space group $R3$ with two protomes in the asymmetric unit and cell dimensions of $a = 114.84$, $b = 114.84$, $c = 191.57$ Å, $\alpha = \beta = 90°$, and $\gamma = 120°$ (hexagonal obverse setting). The structure was solved by using the molecular replacement method implemented in the program X-PLOR (10). The refined crystal structure of a protomer of the proglycinin A1aB1b homotrimer was used as the probe structure (PDB ID code 1FXZ). The cross-rotation search was carried out by using the Patterson search procedures, and the PC refinement of the peak list of the rotation function was performed. The translation function search with the structure corresponding to the highest peak of correlation coefficient 0.118 yielded an outstanding peak at 9.2σ [translation function, $(TF) = 0.250$]. The second molecule was determined by applying the noncrystallographic symmetry obtained from self-rotation function search with an outstanding peak of 10.0σ ($TF =$

PLANT BIOLOGY
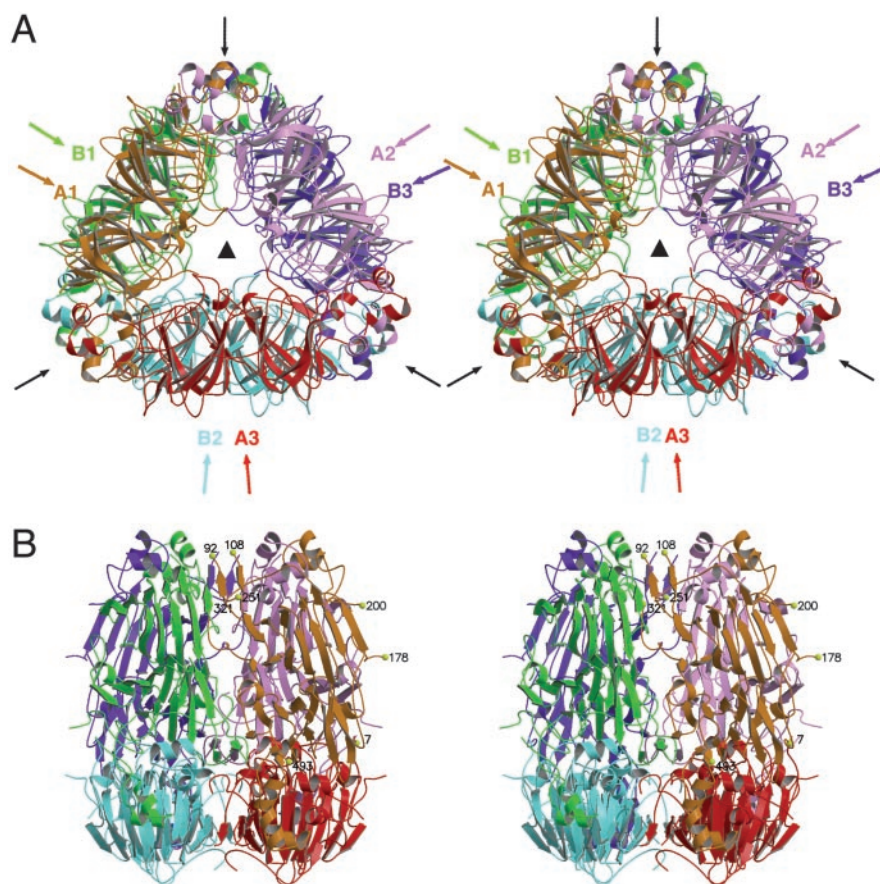
Fig. 1. Stereoviews of the ribbon diagram. Six protomers in the glycinin hexamer are shown in orange (A1), pink (A2), red (A3), green (B1), cyan (B2), and dark blue (B3). (*A*) The threefold axis runs perpendicular to the paper and is shown by a filled triangle. Black arrows indicate the twofold axis of hexamer. Colored arrows indicate pseudo-twofold axis of two trimers composed of A1–A3 and B1–B3. The angle between the red and cyan arrows is 5° when the two arrows (for example, A3 and B2) are projected on a face perpendicular to the paper. (*B*) Ribbon drawing of the hexamer as described for *A* rotated about the vertical axis. Terminal residues of modeled regions in protomer A1 are labeled. The C^α atoms of the terminal residues are represented by yellow spheres. The model was generated by using the programs MOLSCRIPT (23), RASTER3D (24), and PHOTOSHOP (Adobe Systems, Mountain View, CA).

0.253). The relative z translation between two molecules was determined by using combined $TF = 0.631$. Model building and refinement were performed by using the programs TURBO and X-PLOR, respectively.

Calculation of Accessible Surface and Electrostatic Potential. The accessible surface was calculated by using the program NACCESS (11). The probe is taken to be a water molecule as a sphere with a radius of 1.4 Å. Electrostatic surface potential was calculated by using the program GRASP (12). The parameter of salt concentration was changed to 0.1 M from the default setting. The file of full.crg was used for charge assignment, where the histidine residue has no charge. To test the effect of histidine residues, the charge of $N^{\delta 1}$ and $N^{\epsilon 2}$ atoms in histidine residues was set as 0.5.

Results and Discussion

The Overall Structure of Glycinin A3B4 Homohexamer. The crystal structure of the glycinin A3B4 homohexamer was determined at 2.1-Å resolution. The hexamer has 32-point group symmetry and consists of two trimers composed of protomers A1–A3 and B1–B3, respectively, as shown in Fig. 1*A*. A Ramachandran plot of the main-chain conformation angles showed that 87.0% lie within the most favored region, with 100% lying within the allowed region (13). The data collection and refinement statistics are listed in Table 1. Each protomer consists of four visible regions (382 amino acid residues) and four disordered regions (residues 1–6, 93–107, 179–

Table 1. Statistics of data collection and refinement

Data collection	
No. of crystals used	1
Resolution range, Å	44.3–2.1
No. of measured reflections	227,710 (12,780)*
No. of unique reflections	55,186 (5,597)
R_{sym}, %	8.0 (44.7)
Completeness, %	100 (100)
Multiplicity	4.13 (2.28)
$\langle I/\sigma I \rangle$	14.25 (1.92)
Refinement	
Resolution range, Å	10.0–2.1
No. of reflections used, $F > 0$	48,190
No. of residues	1,128
No. of water molecules	214
Average B factor, Å²	
Protein atoms	22.8
Water molecules	31.4
rms deviation	
Bond length, Å	0.013
Bond angle, °	3.1
R factor	0.201 (0.301)
Free R factor†	0.254 (0.356)

*Statistics for outer shells from 2.175 to 2.100 Å.
†Free set contains 10% of reflections.

Adachi *et al.*
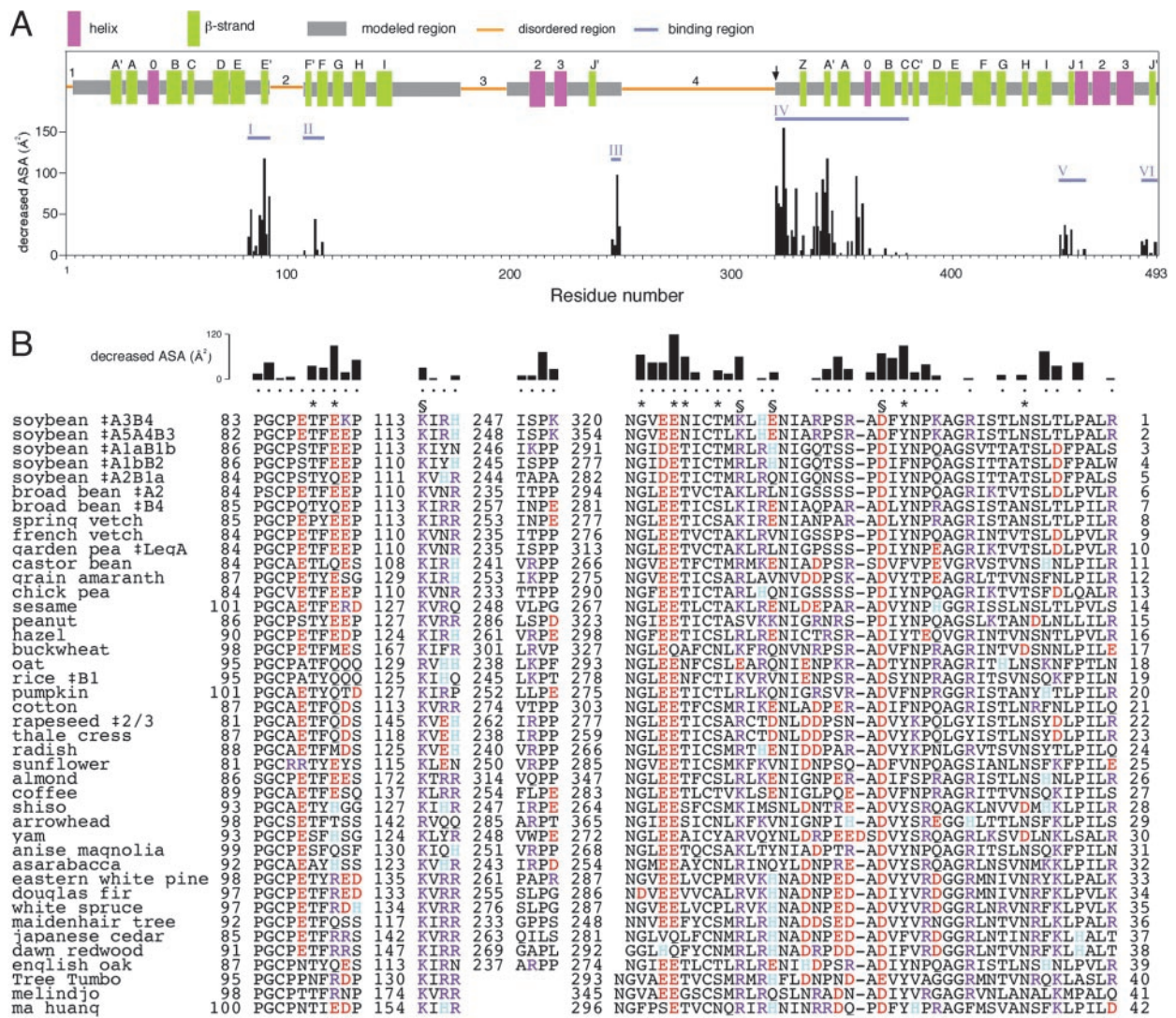
Fig. 2. Binding regions. (*A*) The decrease in ASA by hexamer formation. Secondary structures are indicated at the top. The arrow indicates the processing site between Asn-320 and Gly-321. (*B*) Sequence alignment of the 11S globulin family at the four binding regions. The ‡ indicates the kind of subunit. Basic (Arg and Lys), acidic (Glu and Asp), and histidine residues are shown in blue, red, and cyan, respectively. * and § indicate residues involved in hydrogen bonds and hydrogen-bonded salt bridges, respectively. Filled circles represent residues involved in the decrease of accessible surface. The alignment shows only binding regions in the IE face. The amino acid number is indicated at the left side of the sequence without the signal peptide predicted by SIGNALP (25). The sequence number is shown at the right side of the binding-region IV. The GenBank accession numbers and Latin names are: 1, AB049440, *Glycine max*; 2, X52863, *G. max*; 3, M36686, *G. max*; 4, X15123, *G. max*; 5, D00216, *G. max*; 6, X55014, *Vicia faba*; 7, X03677, *V. faba*; 8, Z32796, *Vicia sativa*; 9, Z46803, *Vicia narbonensis*; 10, X17193, *Pisum sativum*; 11, AF262998, *Ricinus communis*; 12, X82121, *Amaranthus hypochondriacus*; 13, Y15527, *Cicer arietinum*; 14, AF240004, *Sesamum indicum*; 15, AF125192, *Arachis hypogaea*; 16, AF449424, *Corylus avellana*; 17, AF152003, *Fagopyrum esculentum*; 18, X17637, *Avena sativa*; 19, X54314, *Oryza sativa*; 20, M36407, *Cucurbita pepo*; 21, M69188, *Gossypium hirsutum*; 22, X59294, *Brassica napus*; 23, M37247, *Arabidopsis thaliana*; 24, X59808, *Raphanus sativus*; 25, M28832, *Helianthus annuus*; 26, X78119, *Prunus dulcis*; 27, AF054895, *Coffea arabica*; 28, AF180392, *Perilla frutescens*; 29, Y09116, *Sagittaria sagittifolia*; 30, X95510, *Dioscorea caucasica*; 31, X82464, *Magnolia salicifolia*; 32, X95508, *Asarum europaeum*; 33, Z11486, *Pinus strobus*; 34, L07484, *Pseudotsuga menziesii*; 35, X63192, *Picea glauca*; 36, Z50778, *Ginkgo biloba*; 37, X95542, *Cryptomeria japonica*; 38, X95544, *Metasequoia glyptostroboides*; 39, X99539, *Quercus robur*; 40, Z50780, *Welwitschia mirabilis*; 41, Z50779, *Gnetum gnemon*; 42, Z50777, *Ephedra gerardiana*.

199, and 252–320) (Fig. 2*A*), these regions being identical in the two asymmetric protomers. The rms deviation of Cα atoms between the two protomers in the asymmetric unit was 0.28 Å.

Each protomer contains 27 strands and 7 helices (Fig. 2*A*) and is folded into two jelly-roll β-barrel domains and two helix domains. The structure of the mature A3B4 protomer is basically very similar to that of the pro-A1aB1b protomer, although there are some differences in the secondary structural assignment and length of the modeled region. The two protomers are superimposed with an rms deviation of 0.8 Å between the Cα atoms.

Hexamer Formation. The two faces perpendicular to the threefold axis in the trimer were conveniently termed the interchain disulfide-containing (IE) and intrachain disulfide-containing (IA) faces based on the position of the inter- and intrachain disulfide bonds, respectively, which are conserved among members of the 11S globulin family (7). According to the distribution of hydrophobic residues on the surfaces and the position of the processing site, the three-dimensional structure of the A1aB1b homotrimer suggested that interactions might occur between the IE faces to form a mature hexamer. In this study, the crystal structure clearly showed that the hexamer is formed by stacking on the IE face of the trimers along the c axis (the trimers are not in contact via their IA face along the c axis). Here, we describe the ingenious face-to-face mechanism that controls the hexamer formation based on the structures of both

the proglycinin A1aB1b and mature glycinin A3B4. The proglycinin A3B4 homotrimer has a mobile disordered region composed of 74 amino acid residues (residues 252–325) on the IE face. Probably, other 11S globulins also have the mobile region on the IE face, although the length of the regions is variable. The mobile regions will inhibit the formation of the hexamer by steric hindrance, because they are localized on the IE face of the trimer. Although the trimer molecules are synthesized in the endoplasmic reticulum and delivered to the PSV in cells, the cleavage between conserved Asn-320 and Gly-321 residues occurs by a processing enzyme (8, 14). After this cleavage, the disordered regions can move from the IE face to the side of the trimer, because one end of the mobile region is disconnected from the IE face, and the other end can act as a hinge. This process will sufficiently expose the IE face to the solvent. Because the steric hindrance has been removed, the two processed trimers assemble to form the hexamer and eventually lead to the storage of mature 11S globulins in the PSV.

When the structure of proglycinin is compared with that of mature glycinin, two significant differences are found. In the structure of proglycinin A1aB1b, five residues from Gly-292 to Thr-296 just after the processing site were found to be disordered despite their being highly conserved among 11S globulins (Fig. 2B). The electron density maps of the corresponding five residues in the A3B4 hexamer (Gly-321–Asn-325) were clearly visible. The five residues were sandwiched between the two trimers in the hexamer (Fig. 1B). In particular, the accessible surface area (ASA) of Glu-324 is dramatically decreased by the hexamer formation (Fig. 2). The side chain of Glu-324 protrudes from the IE face into the other trimer and makes two hydrogen bonds with Val-451 and Ser-452 and electrostatic interaction with Lys-445 at a distance of 5Å (Fig. 3A). The residue Gly-321 is located near the solvent compared with Glu-324 and has an ASA of only 8 Å^2 as a result of hexamer formation, representing a decrease in ASA of 85 Å^2 (Fig. 2). It seems to be impossible to accommodate even one upstream residue (Asn-320) without steric constraint because of a loop between strand J′ and helix 3 of the next trimer (Fig. 3B). In other words, connections of the Gly residues with any short and long disordered regions will disturb formation of the hexamer, which indicates that the processing of the 11S globulin may be a prerequisite for the 11S globulin to form a hexamer molecule. However, the position of the processing site is not conserved in some gymnosperm 11S globulins (Fig. 2B, 40–42; ref. 15). The structure of these globulins must be different around the twofold symmetry axis to accommodate the longer sequence.

The second difference is that the disordered region 2 of mature glycinin is shorter than the corresponding disordered region of the proglycinin (7). Two new β-strands (E′ and F′) are observed at both sides of region 2 in the mature glycinin hexamer (Fig. 2A). The two strands form a sheet in antiparallel, which stacks on the sheet of the barrel in the C-terminal module of the next protomer, while strand E′ makes interactions with strand A′ as a parallel sheet (Fig. 3C). We conclude that these two structural differences result from the hexamer formation.

Interactions Between Two Trimers. The trimer has an ASA of 12,900 Å^2 when isolated from the hexamer but an ASA of 10,600 Å^2 when within in the hexamer. Sixty-eight residues contributed to this decrease and were classified into six binding regions as shown in Fig. 2A. The four binding regions from I to IV are positioned at both sides of disordered regions 2 and 4, whereas regions V and VI are located near the C-terminal helix region (Fig. 2A). Binding-region IV includes 34 residues and contributes to the 64% decrease in ASA. The level of homology in regions V and VI was low. The results around the strictly conserved Cys-85 in binding-region I are located near the twofold symmetry axis and have van der Waals contacts between protomers A1 and B3, A2 and B2, and A3 and B1.

Twenty-five hydrophobic residues in the binding regions oc-
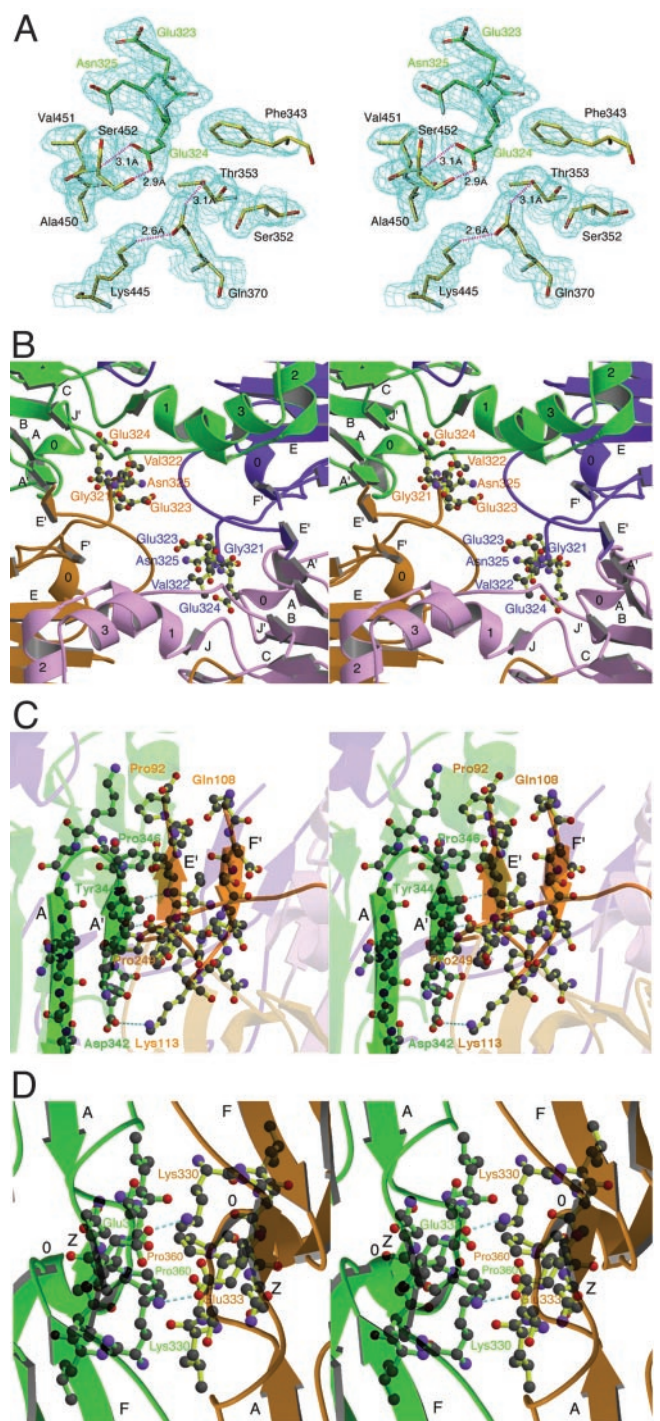
Fig. 3. Interactions between two trimers. Colors of the ribbon model correspond to those in Fig. 1. (A) The 2Fo − Fc electron density map around Glu-324 just after the processing site. The hydrogen bonds are represented by a dotted pink line. (B) Region just after the processing site. The view point is positioned near the head of the black arrow at the top in Fig. 1A. Residues from Gly-321 to Asn-325 are represented by a ball-and-stick model. (C) Ribbon and ball-and-stick models. The atoms that form stacked sheets are represented by using a ribbon and ball-and-stick model. Four strands in the stacked sheets are labeled by black letters. Hydrogen bonds between the two trimers are represented by a dotted cyan line. (D) Hydrogen-bonded salt bridge between Lys-330 and Glu-333. The hydrogen bond is shown by a cyan dotted line. The twofold axis of the hexamer runs perpendicular to the paper in the center on B and D.
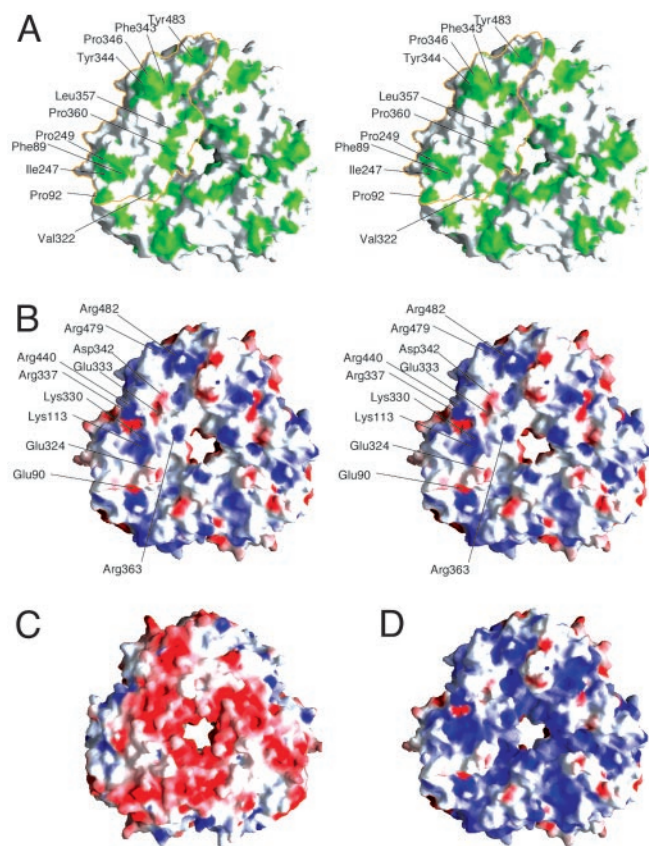
Fig. 4. Distribution of hydrophobic residues and electrostatic surface potential of the A3B4 trimer. The electrostatic potential surface is colored in the range from $-10k_BT$ (red) to $+14k_BT$ (blue), where k_B is the Boltzmann's constant and T is the absolute temperature (in K). (*A*) Stereodiagram of hydrophobic residues on the IE face. Ala, Val, Leu, Ile, Met, Pro, Phe, Tyr, and Trp are colored in green, and the boundary of the protomer is shown in orange. (*B*) Stereodiagram of the electrostatic surface potential of the IE face. Histidine residues are not charged. (*C*) Electrostatic surface potential of the IA face. (*D*) Electrostatic surface potential of the IE face. The histidine residues are positively charged.

cupy an area of 940 Å², corresponding to 40% of the full decrease in ASA. The nine residues Phe-89, Pro-92, Pro-249, Val-322, Phe-343, Tyr-344, Pro-346, Leu-357, and Pro-360 significantly contribute to the decrease in ASA (Figs. 2 and 4*A*). In particular, Phe-89, Pro-249, Val-322, Phe-343, and Pro-360 are highly conserved among members of the 11S globulin family (Fig. 2*B*). Leu-357 and Pro-360 are located on loop AO (residues 354–360) near the twofold symmetry axis, whereas Pro-360 is in close contact with the corresponding residue between protomers A1 and B1, A2 and B3, and A3 and B2 (Fig. 3*D*). Pro-249 is positioned just before the biggest disordered region on the surface of the hexamer, and Pro-249 interacts with Tyr-344 of the next protomer by van der Waals contact. The aromatic ring of Tyr-344 is inserted between two pyrrolidine rings of the proline residues (Fig. 3*C*). In addition, Phe-343 interacts with Val-322 near the stacking site. It seems that these hydrophobic interactions are very important for formation of the hexamer.

Thirty hydrogen bonds and two hydrogen-bonded salt bridges

are assigned between two stacked protomers. However, we could not find any hydrogen bonds between protomers A1 and B2 or A1 and B3. Lys-113 and Lys-330 formed hydrogen-bonded salt bridges with Asp-342 and Glu-333, respectively (Fig. 3 *C* and *D*). The distances between N^ζ of Lys-113 and $O^{\delta 2}$ of Asp-342 and between $O^{\epsilon 1}$ of Glu-333 and N^ζ of Lys-330 are the same: 2.9 Å. The two residues Lys-113 and Asp-342 are strictly conserved among members of the 11S globulin family (Fig. 2*B*), and the hydrogen-bonded salt bridge between them probably plays a key role in the binding of the two trimers.

Favorable electrostatic attraction is recognized as a driving force for fast association of protein–protein interaction (16, 17), and the pH will change according to sorting from the endoplasmic reticulum (pH 7.4) (18) to the PSV (pH 6.0) (19). We therefore calculated the electrostatic potential on the IE and IA faces of the trimer. The results show that the IE face is slightly positive (Fig. 4*B*), whereas the IA face carries a highly negative charge (Fig. 4*C*). The mobile region of soybean glycinin includes many acidic residues, which may prevent random association of proglycinins through interaction between the IA and IE faces. After exposure of the IE face to the solvent in the PSV by processing, it appears that the negative and positive charges are effectively distributed to favor the formation of the hexamer, and a similar distribution is also found on the IE face of the A1aB1b homotrimer. It is likely that this charge distribution is responsible for the association of the hexamer with hydrophobic interactions and short-range specific interactions such as hydrogen bonds, van der Waals contact, and hydrogen-bonded salt bridges in the PSV. Lys-113 and Asp-342 may make specific long-range charge–charge interactions. In addition, the hydrophobic residues of Pro-249 and Tyr-344 located on the side of the IE face would be able to interact with each other. These residues may contribute to the association of the trimers through nonspecific hydrophobic interactions in the transition state (17).

Degradation of 11S Globulin at the Stage of Germination. During germination and seedling growth, storage proteins are degraded and mobilized (20), and it is possible that they become unstable as a result of the change of conditions during these stages. For example, the pH in vacuoles decreases from 6.0 to 5.5 during germination (19). Although the conditions required for dissociation are different among proteins, the dissociation from 11S hexamer to 7S trimer occurs after changing the pH and/or ionic strength (21, 22). At acidic pH, the histidine residues exhibit a positive charge, which results in the IE face becoming more positively charged (Fig. 4*D*). The distribution of the charges suggests that the electrostatic potential might result in dissociation due to the repulsion between positively charged IE faces. Furthermore, the electrostatic interaction would be more effective at lower ionic conditions after imbibition. After the dissociation from a hexamer to a trimer, the dissociated trimer will have more flexible mobile regions than the pro form and be more susceptible to proteinases. This mechanism may contribute to the degradation of 11S globulins during germination and seedling growth.

1. Utsumi, S. (1992) *Adv. Food Nutr. Res.* **36,** 89–208.
2. Shewry, P. R. (1995) *Biol. Rev.* **70,** 375–426.
3. Shutov, A. D. & Bäumlein, H. (1999) in *Seed Proteins,* eds. Shewry, P. R. & Casey, R. (Kluwer, London), pp. 543–561.
4. Lawrence, M. C., Izard, T., Beuchat, M., Blagrove, R. J. & Colman, P. M. (1994) *J. Mol. Biol.* **238,** 748–776.
5. Ko, T. P., Day, J. & McPherson, A. (2000) *Acta Crystallogr. D* **56,** 411–420.
6. Maruyama, N., Adachi, M., Takahashi, K., Yagasaki, K., Kohno, M., Takenaka, Y., Okuda, E., Nakagawa, S., Mikami, B. & Utsumi, S. (2001) *Eur. J. Biochem.* **268,** 3595–3604.
7. Adachi, M., Takenaka, Y., Gidamis, A. B., Mikami, B. & Utsumi, S. (2001) *J. Mol. Biol.* **305,** 291–305.

8. Dickinson, S. D., Hussein, E. H. A. & Nielsen, N. C. (1989) *Plant Cell* **1,** 459–469.

9. Yagasaki, K., Takagi, T., Sasaki, M. & Kitamura, K. (1997) *J. Agric. Food Chem.* **45,** 656–660.

10. Brünger, A. T. (1993) X-PLOR: A System for X-Ray Crystallography and NMR (Yale Univ. Press, New Haven, CT), Version 3.1.

11. Hubbard, S. J. & Thornton, J. M. (1993) ACCESS (Dept. of Biochemistry and Molecular Biology, University College, London).

12. Nicholls, A., Sharp, K. A. & Honig, B. (1991) *Proteins Struct. Funct. Genet.* **11,** 281–296.

13. Laskowski, R. A., MacArthur, M. W., Moss, D. S. & Thorton, J. M. (1993) *J. Appl. Crystallogr.* **26,** 283–291.

14. Jung, R., Sccot, M. P., Nam, Y. W., Beaman, T. W., Bassüner, R. & Saalbach, I. (1998) *Plant Cell* **10,** 343–357.

15. Wind, C. & Hager, K. P. (1996) *FEBS Lett.* **383,** 46–50.

16. Selzer, T., Albeck, S. & Schreiber, G. (2000) *Nat. Struct. Biol.* **7,** 537–541.

17. Schreiber, G. (2001) *Curr. Opin. Struct. Biol.* **12,** 41–47.

18. Wu, M. M., Grabe, M., Adams, S., Tsien, R. Y., Moore, H. P. H. & Machen, T. E. (2001) *J. Biol. Chem.* **276,** 33027–33035.

19. Okamoto, T., Yuki, A., Mitsuhashi, N. & Minamikawa, T. (1999) *Eur. J. Biochem.* **264,** 223–232.

20. Müntz, K., Belozersky, M. A., Dunaevsky, Y. E., Schlereth, A. & Tiedemann, J. (2001) *J. Exp. Bot.* **52,** 1741–1752.

21. Utsumi, S., Matsumura, Y. & Mori, T. (1997) in *Food Proteins and Their Applications*, eds. Damodaran, S. & Paraf, A. (Dekker, New York), pp. 257–291.

22. Lakemond, C. M. M., de Jongh, H. H. J., Hessing, M., Gruppen, H. & Voragen, A. G. J. (2000) *J. Agric. Food Chem.* **48,** 1985–1990.

23. Kraulis, P. (1991) *J. Appl. Crystallogr.* **24,** 946–950.

24. Meritto, E. A. & Murphy, M. E. P. (1994) *Acta Crystallogr. D* **50,** 869–873.

25. Nielsen, H., Engelbrecht, J., Brunak, S. & von Heijne, G. (1997) *Protein Eng.* **10,** 1–6.